Optimal Frequency for Wireless Power Transmission Into the Body: Efficiency Versus Received Power

Daniel K. Freeman and Steven J. Byrnes

***Abstract*— Wireless power delivery to implantable devices has been traditionally achieved through low-frequency (<10 MHz) inductive coupling. More recent work has moved toward the UHF band (300 MHz–3 GHz), with models showing maximal efficiency is achieved at these frequencies. However, for many applications, maximizing efficiency is a secondary goal to maximizing received power at the implant, and it remains unclear whether the optimal frequency for efficiency is different than the optimal frequency for maximizing received power. Furthermore, previous models generally do not include a ferrite core in the implant, which could shift the optimal frequency. To address these questions, we developed a theoretical model with frequency-dependent ferrite permeability and dispersive tissue. We show that when a ferrite core is included, the optimal frequency for efficiency remains in the UHF band. Conversely, when maximizing received power rather than efficiency, both high (>300 MHz) and low (<10 MHz) frequencies yield similar levels of received power, and this remains true with or without a ferrite core. For shallow implants, heating of the core can reach unsafe levels when operated in the UHF band at field levels approaching the specific absorption rate (SAR) limit. These results have implications for a wide range of medical applications, including sub-millimeter-sized implants and fast recharge of implantable batteries.**

***Index Terms*— Ferrite core, implantable devices, wireless power.**

I. Introduction

IN ORDER to effectively deliver wireless power to medical implants, it is important to understand how electromagnetic fields interact with biological tissue. In particular, tissue heating plays an important role because: 1) such heating sets the upper limit of field levels that can be applied to the body and 2) such heating necessarily involves energy that is drawn from the transmitter, and thus will reduce the efficiency of the link. The most common form of wireless power delivery to implanted devices is low-frequency inductive coupling (<10 MHz) because of the ability of electromagnetic fields to penetrate the body with little tissue heating at these low frequencies [1]–[4]. More recently, there has been a shift toward higher frequencies because of advantages that include less orientation sensitivity and smaller, more efficient transmitters [5], [6]. Indeed, modeling and experimental results suggest that the optimal frequency for efficient wireless power transfer into the body is generally in the UHF band (300 MHz–3 GHz), despite the propensity for tissue heating at these frequencies [7]–[9].

However, the optimal frequency for maximizing efficiency may not be the same as the optimal frequency for maximizing the power received at the implant. For example, when maximizing efficiency, the optimal frequency is one in which the total heat dissipated over all the tissue is low compared to the power received at the implant. Conversely, when maximizing received power, the applied field levels are increased as large as possible until some local hotspot exceeds the safety limits set forth by the FCC. Thus, the optimal frequency for maximizing received power may or may not be efficient, depending on the spatial pattern of the heating in the tissue.

The question of whether to maximize efficiency or received power will depend on the application. Efficiency is important, for example, with battery-powered transmitters where higher efficiency will extend the lifetime of a hand-held transmitter. Conversely, if the transmitter is being used to recharge an implantable battery, then increasing the efficiency of the link may be a secondary goal to maximizing the amount of power that can be received at the implant without exceeding safety limits, thus allowing the recharge to happen as quickly as possible, perhaps even at the expense of efficiency. Likewise, if the goal is to make the implant extremely small (<1 mm^3), then maximizing the received power may take priority over efficiency [10]. Here, we aim to delineate these two competing goals by estimating the optimal frequency for maximizing efficiency as compared to maximizing received power.

Another issue that we aim to address here is that previous models generally do not examine the effect of using a magnetic core in the implanted coil, which can be used to increase power transfer [11], [12]. This raises the possibility that the inclusion of a magnetic core would shift the optimal frequency for wireless power transfer. At the mains frequency (50–60 Hz), this typically involves cores made from iron alloys. At higher frequencies, the eddy current losses in iron cores become too high, necessitating the use of ferrite cores. Ferrites are ferrimagnetic, iron oxide-based ceramics exhibiting high resistivity and moderate levels of permeability. At radio frequencies, ferrites exhibit hysteresis, which for power applications typically confines their use to frequencies of <10 MHz in order to maintain efficiency [13]. However, for wireless power delivery

Manuscript received September 10, 2018; revised October 31, 2018; accepted March 6, 2019. Date of publication March 18, 2019; date of current version May 31, 2019. *(Corresponding author: Daniel K. Freeman.)*

The authors are with the Charles Stark Draper Laboratory, Inc., Cambridge, MA 02139 USA (e-mail: danielkfreeman@gmail.com).

Color versions of one or more of the figures in this paper are available online at http://ieeexplore.ieee.org.

Digital Object Identifier 10.1109/TAP.2019.2905672

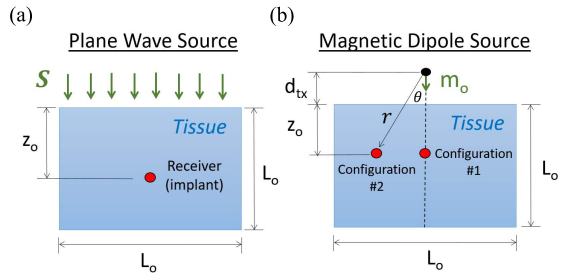

Fig. 1. (a) Model consisting of an implanted receiver coil that is embedded in biological tissue where the source is a plane wave, represented by the Poynting vector, S. (b) Magnetic dipole source positioned at a distance d_{tx} above the surface of the tissue, for the two different implant locations: Configurations #1 and #2. Spherical coordinates are used to represent the position of the implant, with the r- and θ-dimensions shown, and the ϕ-dimension measuring the angle out-of-plane. For both the plane wave and magnetic dipole source, the volume of tissue is $L_o \times L_o \times L_o$, where $L_o = 10$ cm. The tissue properties are assumed to be homogeneous.

to implantable devices, it is possible that core loss associated with hysteresis is negligible compared to the power dissipated in the tissue. If so, ferrites could be operated at much higher frequencies (e.g., in the UHF band) without reducing the efficiency. In addition, it remains unclear whether the heating associated with core loss would reach unsafe levels when operating at the highest allowable field levels as set by the FCC-limited specific absorption rate (SAR) [14]. Our goal was to develop a model that would allow us to quantify the impact that a ferrite core will have on both performance and safety.

One of the reasons that optimizing the frequency of wireless power transmission into the body continues to be an evolving area of research is that biological tissue exhibits complex electrical properties [15]–[18]. This complexity derives from the many polarization processes that exist in tissue, and particularly, the frequency dependence of this polarization (i.e., dispersion). This frequency-dependent polarization necessarily has some loss associated with it, and as a result, energy from electromagnetic fields is dissipated in the tissue as heat. These loss mechanisms have been well-understood for decades [19], but they are often not accounted for in older models of wireless power transfer [20]–[23]. More recent models of wireless power transfer have taken into account the dispersive properties of biological tissue, including both analytical modeling and finite element modeling [8], [9]. We sought to extend the results of these models by assessing the impact of a ferrite core on the optimal frequency for wireless power delivery.

In order to assess the optimal frequency for efficiency as compared to received power, we developed a simple analytical model that takes into account the dispersive nature of biological tissue, the frequency dependence of ferrite permeability, and the maximum field levels that can be applied to the body, as set by the SAR. We consider the source to be either a plane wave or a magnetic dipole [Fig. 1(a) and (b)], and we considered different types of biological tissues. The modeling results suggest that the inclusion of a ferrite core will: 1) increase the peak levels of efficiency and power transfer that can be achieved; 2) generally exhibit the peak efficiency in the UHF band, depending on tissue type; 3) exhibit peak power that does not show a clear optimal frequency when using a magnetic dipole source, which accounts for both the evanescent and radiating fields; and 4) exhibit levels of heating that in some cases could be unsafe for the surrounding tissue, and particularly, for shallow implants at frequencies in the UHF band for field levels approaching the SAR limit. To avoid such heating, ferrite cores can be powered at lower frequencies (<10 MHz). To assess the optimal design for cases where heating is a concern (shallow implants and high fields), we compared the performance of a ferrite core operated at 10 MHz to an air core at 1 GHz, and we find that the ferrite core can achieve higher power levels, while the air core achieves higher efficiency.

II. Methods

A. Model for Dispersive Tissue Loss in Biological Tissue

When an electric field impinges on a polarizable material such as biological tissue, there will be some charge that is induced. The appearance and disappearance of this charge with an oscillating electric field constitutes a displacement current (in time-harmonic form)

$$J = j\omega\epsilon E \tag{1}$$

where ϵ is the permittivity defined as $\epsilon = \epsilon^*\epsilon_o$, and ϵ_o and ϵ^* are the permittivity of the free space and the complex relative permittivity of the tissue, respectively. The biological tissue is often modeled with a slight variation of the Debye model known as the Cole–Cole model. We will use a four-term Cole–Cole model

$$\epsilon^* = \sum_{n=1}^{4}\left[\epsilon_\infty + \frac{\Delta\epsilon_n}{1+(j\omega\tau_n)^{(1-\alpha)}}\right] + \frac{\sigma_{DC}}{j\omega\epsilon_o} \tag{2}$$

where the ϵ_∞, τ_n, $\Delta\epsilon_n$, α, and σ_{DC} were taken from [15] for muscle, skin (dry), brain (gray matter), and blood. Using the typical nomenclature of lossy dielectric materials, the dc conductivity of the tissue, σ_{DC}, is accounted for in the expression for permittivity, even though it represents a true ohmic current ($J = \sigma_{DC}E$) that is distinct from the polarization processes. Expressing the current in terms of ϵ^*

$$J = j\omega\epsilon E = E\left[j\omega\epsilon_o\sum_{n=1}^{4}\left(\epsilon_\infty + \frac{\Delta\epsilon_n}{1+(j\omega\tau_n)^{(1-\alpha)}}\right)+\sigma_{DC}\right] = \sigma^* E. \tag{3}$$

The expression in brackets is complex and frequency dependent, and it is often referred to as the complex conductivity σ^*. The imaginary part of σ^* describes the component of J and E that are 90° out-of-phase, exhibiting purely reactive behavior where no energy is dissipated in the tissue. The real part of σ^* describes the component of J and E that are in-phase, where energy is dissipated in the tissue as heat. This loss term is often referred to as the effective conductivity of the material

$$\sigma_e = \mathrm{Re}\left[\sigma^*\right]. \tag{4}$$

By convention, the reactive component is not defined in terms of the imaginary part of σ^*, but rather in terms of the frequency-dependent permittivity ϵ'

$$\epsilon' = \mathrm{Re}[\epsilon^*] = \frac{\mathrm{Im}[\sigma^*]}{\omega\epsilon_o}. \tag{5}$$

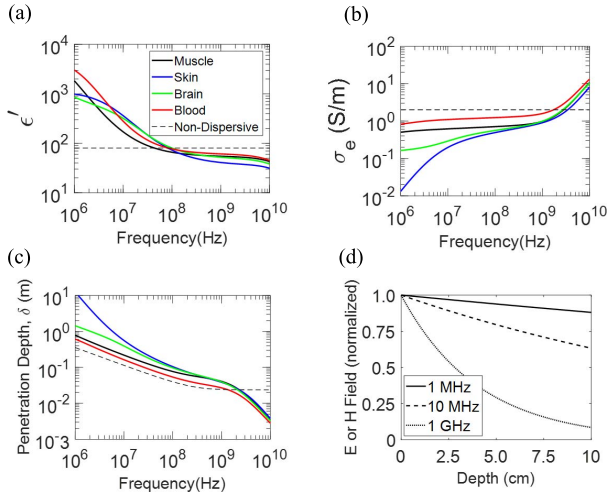

Fig. 2. (a) Frequency-dependent permittivity and (b) effective conductivity for several types of tissue, based on the Cole–Cole model with parameters derived from [15]. (c) Penetration depth versus frequency for a range of tissue types. (d) Penetration of the E-field and H-field into tissue at 1 MHz, 10 MHz, and 1 GHz. The legend in (a) applies to (b) and (c).

Parameters σ_e and $\epsilon^{'}$ are commonly plotted as a function of frequency when characterizing the electrical properties of biological tissue [15]–[18], [24]. We plot some examples of permittivity and conductivity for a model that was fitted to real biological tissue. Permittivity $\epsilon^{'}$ decreases significantly with increasing frequency, while conductivity σ_e increases with frequency for a variety of biological tissues [Fig. 2(a) and (b)]. To illustrate the effect of the dispersive properties of tissue, we will also consider a nondispersive medium that is characterized by frequency-independent values of permittivity ($\epsilon^{'} = 80$) and conductivity ($\sigma_e = 2\mathrm{S/m}$).

B. Penetration of Electromagnetic Waves Into the Tissue

The ability of electromagnetic fields to penetrate biological tissue will depend on the dc conductivity of the tissue, as well as any dispersive losses associated with polarization. Both of these loss mechanisms are accounted for in the frequency-dependent conductivity σ_e. Assuming the far-field conditions, we can use the expression for penetration depth [25] to estimate the level of penetration across the frequency

$$\delta = \left(\mathrm{Im}\left[\frac{\omega\sqrt{\epsilon}^*}{c}\right]\right)^{-1} = \left(\omega\sqrt{\frac{\epsilon^{'}\epsilon_o\mu_o}{2}}\left[\sqrt{1+(\frac{\sigma_e}{\epsilon^{'}\epsilon_o\omega})^2}-1\right]^{1/2}\right)^{-1}. \quad (6)$$

The permeability of the tissue is assumed to be equivalent to that of free space μ_o. The penetration depth is shown as a function of frequency for different types of tissue [Fig. 2(c)], yielding larger penetration depths for lower frequency, as expected. We assume a plane wave with uniform fields in the x–y dimensions. If we define the magnetic field intensity at the surface of the tissue as H_s, then the magnetic field within the tissue at a depth z from the tissue surface can be expressed as

$$H(z) = H_s e^{-z/\delta}. \quad (7)$$

An analogous expression exists for the electric field $E(z)$, where the electric field at the surface of the tissue is defined as E_s, and the amplitude decays exponentially as a function of depth. The penetration of electric and magnetic fields is shown in Fig. 2(d), yielding significant penetration at low frequencies (<10 MHz).

C. Properties of the Ferrite Core

Magnetic cores can be characterized by their permeability, which is a measure of the extent to which the material becomes magnetized when a magnetic field is applied. As with the permittivity, the permeability is frequency dependent, with maximal permeability at low frequencies, and lower permeability at higher frequencies. We will consider ferrite cores, which exhibit relative permeability on the order of 10–100 at low frequencies [26]. To describe the frequency dependence, we introduce the complex permeability μ^*

$$\mu^* = \mu^{'} + j\mu^{''} \quad (8)$$

where $\mu^{'}$ and $\mu^{''}$ are the real and imaginary parts of the complex relative permeability, respectively. The total magnetic flux can be quantified by a total permeability μ given by

$$\mu = \mu_{\mathrm{eff}}\mu_o \quad (9)$$

where μ_o is the permeability of free space, and μ_{eff} is the effective relative permeability, defined as

$$\mu_{\mathrm{eff}} = \frac{\mu^*}{1+N(\mu^*-1)} \quad (10)$$

where μ_{eff} is generally less than μ^* because the magnetized core will generate H-fields that are antiparallel to the applied field [27]–[29]. This demagnetizing field is proportional to the magnetization of the core by the geometry-dependent demagnetization factor, N[30]. We will consider a cylindrical core, where the demagnetization factor can be approximated as

$$N = \frac{1}{\left(\frac{4n}{\sqrt{\pi}}\right)+1} \quad (11)$$

where n is the aspect ratio (length/diameter) of the cylinder [31].

Permeability values versus frequency for $\mu^{'}$ and $\mu^{''}$ were extracted from datasheets for a commercially available nickel-zinc ferrite (Fair-Rite #61) [Fig. 3(a)]. The effective permeability is shown for an aspect ratio of 5:1 (N = 0.08), 10:1 (N = 0.04), as well as for the case with no demagnetization (N = 0) [Fig. 3(b)]. The characterization data for most ferrites are available up to 1 GHz, and therefore, all model results presented here that include ferrites will have a maximal frequency of 1 GHz. For the field levels used here, the ferrites will not exhibit saturation. No air gap was assumed between the coil and the ferrite core. Winding losses are not considered here, and the eddy current loss in the core is considered negligible because of the high resistivity of the ferrite ($\approx 10^7\ \Omega\cdot$ cm). Unless otherwise stated, the diameter of the core will be 0.5 mm, and the length of the core will be 2.5 mm.

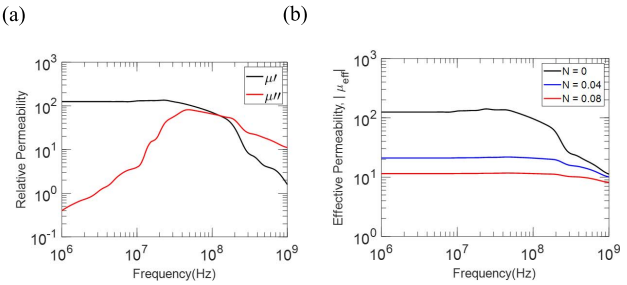

Fig. 3. (a) Real (μ') and imaginary (μ'') parts of the complex permeability, μ^*, for #61 nickel-zinc ferrite. (b) Effective (relative) permeability (μ_{eff}) that results when accounting for the demagnetizing field for a 5:1 and 10:1 aspect ratio ferrite cylinder, yielding N = 0.08 and N = 0.04, respectively, as compared to no demagnetization (N = 0).

III. Results

A. Maximizing Power Transfer to the Implant With a Plane Wave Source

We will consider a plane wave source where the field intensities are uniform across the entire surface of the tissue. The tissue is assumed to be homogenous, with a volume of $L_o \times L_o \times L_o$, where $L_o = 10$ cm [Fig. 1(a)]. The implant will be considered to be at a depth of $z = z_o$, where the surface of the tissue is defined as $z = 0$. Power can be delivered to an implanted coil with an ac magnetic field, which will induce an electromotive force (EMF), V_{emf}, in the implanted coil. For a sinusoidally oscillating magnetic field of frequency, ω, and an implanted coil of area, A_{coil}, the magnitude of the EMF induced in the coil can be expressed as

$$|V_{\text{emf}}| = |\mu\omega H(z_o) A_{\text{coil}}| \tag{12}$$

where $H(z_o)$ is the H-field component normal to the implanted coil at depth z_o, and μ incorporates the complex permeability of the ferrite core. We are assuming a single-turn coil. For coils with N-turns, the induced voltage is increased by a factor of N. The power delivered to the load for a plane wave source is equal to

$$P_{r,p} = \left| \frac{V_{\text{emf}}^2}{2Z_{\text{load}}} \right| \tag{13}$$

where the load is assumed to be conjugate matched such that $Z_{\text{load}} = 50\ \Omega$ (see Section IV). The factor of ½ comes from the fact that V_{EMF} represents the peak amplitude, rather than the rms. In order to maximize the received power, we would like the magnetic field at the implant to be as large as possible until the field levels reach the SAR limit. We will assume that the core loss is negligible, as discussed later. Tissue heating is a function of applied electric field and not the magnetic field, and therefore, we must express the magnetic field at the implant, $H(z_o)$, in terms of the electric field at the surface of the tissue, where the fields are largest. Since we are considering a plane wave, the magnetic field and electric field are related by the wave impedance

$$Z_w = \frac{E_s}{H_s} = \sqrt{\frac{\mu_o}{\epsilon}} \tag{14}$$

where E_s and H_s represent the electric and magnetic fields at the tissue surface, respectively, ϵ incorporates the complex permittivity of the tissue, and μ_o represents the permeability of the tissue, equivalent to free space. Using the wave impedance and the expression for skin depth, we express the magnetic field at depth, z_o, in terms of the electric field at the surface, E_s

$$H(z_o) = \frac{E_s}{\sqrt{\mu_o/\epsilon}} e^{-z_o/\delta}. \tag{15}$$

In order to achieve the maximum power delivered to the implant, the magnetic field is increased until the electric field at the surface reaches its maximum allowable level, $E_s = E_{\max}$. The relationship between the SAR limit, S, and maximum allowed electric field amplitude, $E_{\max}$, is

$$S = \frac{\sigma_e E_{\max}^2}{2\rho} \tag{16}$$

where ρ is the tissue density, approximated as 900 kg/m^3 for soft tissue [32], [33]. We will assume that S is 1.6 W/kg, measured over 1 g of tissue, as set by the FCC for uncontrolled environments [14]. We assume that the magnitude of the electric field over any 1 g of tissue is approximately uniform, and therefore, the SAR limit corresponds to the case where the amplitude of the electric field at any location reaches a value of $E_{\max}$. The magnetic field amplitude at depth z_o can then be expressed in terms of the SAR limit

$$H(z_o) = \frac{E_{\max}}{\sqrt{\frac{\mu_o}{\epsilon}}} e^{-\frac{z_o}{\delta}} = \sqrt{\frac{\epsilon}{\mu_o}} \sqrt{\frac{2S\rho}{\sigma_e}} e^{-\frac{z_o}{\delta}}. \tag{17}$$

We can now express the received power as a function of the frequency-dependent conductivity of the tissue (σ_e), the complex effective permeability of the ferrite core (μ_{eff}), and the SAR limit (S)

$$\begin{aligned} P_{r,p} &= \left| \frac{1}{2|Z_{\text{load}}|} \left(\mu\omega \sqrt{\frac{\epsilon}{\mu_o}} \sqrt{\frac{2S\rho}{\sigma_e}} e^{-\frac{z_o}{\delta}} A_{\text{coil}} \right)^2 \right| \\ &= \frac{(|\mu_{\text{eff}}|\omega)^2 \mu_o |\epsilon| S\rho e^{-\frac{2z_o}{\delta}} A_{\text{coil}}^2}{|Z_{\text{load}}|\sigma_e}. \end{aligned} \tag{18}$$

The received power is plotted in Fig. 4(a) for muscle tissue and a nondispersive medium with no ferrite core. While muscle exhibits a peak at 1–2 GHz [Fig. 4(a)], the nondispersive medium does not exhibit a peak frequency, suggesting that the dispersive properties of tissue are responsible for the optimal frequency of muscle nearly 1 GHz.

The effects of dispersive tissue are further illustrated in Fig. 4(b), showing the maximum allowed H-field that can be achieved at the implant for muscle and a nondispersive medium. For muscle, the peak H-field decreases sharply beyond 2 GHz as a result of the corresponding increase in effective conductivity, producing a decrease in received power at high frequencies. Conversely, the maximum H-field that can be achieved for the nondispersive medium exhibits a plateau beyond 1 GHz, mirroring the plateau in penetration depth at high frequencies [Fig. 2(c)]. These results illustrate the role of dispersive processes in determining the optimal frequency for power transfer.

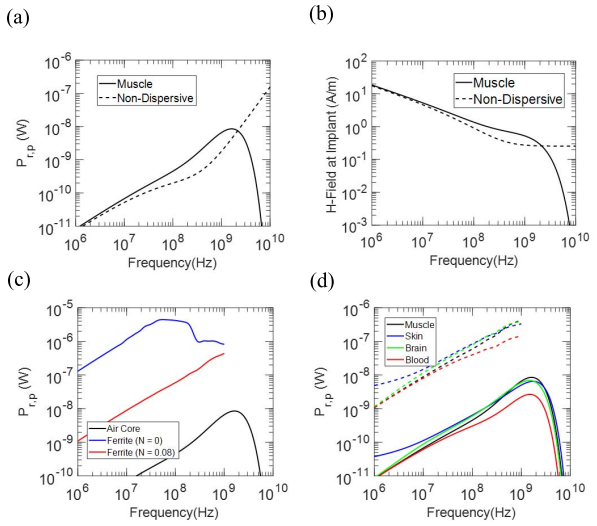

Fig. 4. Received power for a plane wave source. (a) Results for an air core (no ferrite) with dispersive muscle tissue and a nondispersive medium. (b) H-field at the implant when the electric field at the tissue surface is at the SAR limit. (c) Received power for an air core versus a ferrite core for muscle tissue for cases with (N = 0.08) and without (N = 0) demagnetization. (d) Received power for various tissue types with an air core (solid line) versus a ferrite core (dashed line). The implanted coil consists of a single loop with area $A_{coil} = 0.2$ mm^2, and the implant depth in all cases is $z_o = 3$ cm.

Incorporating a ferrite core into the implanted coil causes a significant increase in the power delivered to the load [Fig. 4(c)]. For the case when the demagnetization effects of the core are not accounted for (N = 0), the optimal frequency shifts below 100 MHz. Conversely, when the demagnetization is account for (N = 0.08), the optimal frequency is $\geq$1 GHz, although a peak cannot be resolved because this ferrite is characterized only up to 1 GHz. This illustrates the importance of incorporating the effects of demagnetization into the model. In practice, there will always be some level of demagnetization in the core, and therefore, all subsequent results will consider only the case where demagnetization is accounted for, using N = 0.08 to represent a core with 5:1 aspect ratio.

The effect of including a ferrite core is shown for a range of tissue types, and in all cases, there is a significant increase in power transfer when the core is included [Fig. 4(d)]. The peak power increases by approximately 2 orders of magnitude, consistent with a 1 order of magnitude increase in induced voltage as a result of the effective permeability of $\approx$10 [Fig. 3(b)]. This simple model shows that optimal power transfer is achieved near 1 GHz. However, because the source is a plane wave, any near-field coupling is not accounted for, requiring a modification of the model to include a magnetic dipole source.

B. Maximizing Power Transfer to the Implant With a Magnetic Dipole Source

The analysis shown above for a plane wave source is relatively simple because for a plane wave, the H- and E-fields can be related by the wave impedance, Z_w. In reality, this model is not accurate for sources that consist of transmitter coils positioned close to the tissue, which is more often modeled as a magnetic dipole [Fig. 1(b)]. A magnetic dipole source has a near field whose H/E ratio can be much higher than $1/Z_w$, which is advantageous because the H-field powers the receiver (via the induced EMF in the implanted coil) while the E-field heats the tissue. We can express the H-field vector of a magnetic dipole, in spherical coordinates $(\hat{\boldsymbol{r}}, \hat{\boldsymbol{\theta}}, \hat{\boldsymbol{\phi}})$[34]

$$\boldsymbol{H} = \frac{j\omega\mu_o m_o}{4\pi Z_w}\left\{2\cos(\theta)\left[\frac{1}{r^2} - \frac{j}{\beta r^3}\right]e^{-j\beta r}\hat{\boldsymbol{r}} + \sin(\theta)\left[\frac{j\beta}{r} + \frac{1}{r^2} - \frac{j}{\beta r^3}\right]e^{-j\beta r}\hat{\boldsymbol{\theta}}\right\} \quad (19)$$

where m_o is the amplitude of the magnetic dipole, in units of A·m^2, and $\beta = \omega\sqrt{\mu_o\epsilon}$ is the complex angular wavenumber. Permittivity ϵ incorporates the tissue properties. In the estimate of $\mathbf{H}$, we do not include the properties of air between the transmitter and the tissue surface in order to keep the model analytically tractable (see Section IV). The H-field vector contains no component in the ϕ-direction. Conversely, the electric field associated magnetic dipole has only a component in the ϕ-direction

$$\boldsymbol{E} = \frac{-j\omega\mu_o m_o}{4\pi}\sin(\theta)\left[\frac{j\beta}{r} + \frac{1}{r^2}\right]e^{-j\beta r}\hat{\boldsymbol{\phi}}. \quad (20)$$

We would like to know the amplitude of the magnetic dipole moment, m_o, that will cause the SAR limit to be reached, which occurs when the electric field measured over 1 g of tissue is equivalent to E_{max}. We will assume that the magnitude of the electric field over any 1 g of tissue is approximately uniform. Therefore, we set the magnitude of the electric field equivalent to E_{max}

$$|\boldsymbol{E}| = E_{max} = \sqrt{\frac{2S\rho}{\sigma_e}}. \quad (21)$$

Solving the expression for E in terms of the dipole moment, m_o, we define the signal strength from the transmitter that is necessary to reach the SAR limit

$$m_{o,max} = \left|\frac{-j\omega\mu_o}{4\pi}\sin(\theta)\left[\frac{j\beta}{r} + \frac{1}{r^2}\right]e^{-j\beta r}\right|^{-1}\sqrt{\frac{2S\rho}{\sigma_e}}. \quad (22)$$

We then plug in the expression for $m_{o,max}$ into the expression for $\mathbf{H}$

$$\boldsymbol{H}_{\mathbf{max}} = \frac{j\omega\mu_o m_{o,max}}{4\pi Z_w}\left\{2\cos(\theta)\left[\frac{1}{r^2} - \frac{j}{\beta r^3}\right]e^{-j\beta r}\hat{\boldsymbol{r}} + \sin(\theta)\left[\frac{j\beta}{r} + \frac{1}{r^2} - \frac{j}{\beta r^3}\right]e^{-j\beta r}\hat{\boldsymbol{\theta}}\right\} \quad (23)$$

where $\mathbf{H}_{\mathbf{max}}$ is the magnetic field at the receiver when the intensity of the source is increased to its maximum allowable level, $m_{o,max}$. The power at the receiver for a magnetic dipole source, as measured at the SAR limit, can then be defined as

$$P_{r,d} = \left|\frac{\left(\mu\omega(\boldsymbol{H}_{\mathbf{max}}\cdot\hat{\boldsymbol{n}})A_{coil}\right)^2}{2Z_{load}}\right| \quad (24)$$

where $\hat{n}$ is a unit-length vector that is normal to the plane of the implanted coil. The factor of 1/2 comes from the fact that

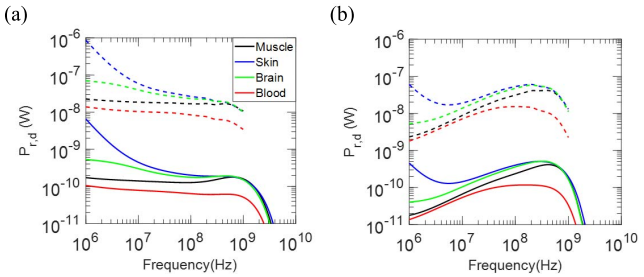

Fig. 5. (a) and (b) Received power for a magnetic dipole source for various tissue types with a ferrite core (dashed line) and with an air core (solid line). Results are shown for Configuration #1 in (a) and Configuration #2 in (b). The implant coil is a single loop with area $A_{coil} = 0.2$ mm^2, and the demagnetization factor is N = 0.08.

the field levels are represented in peak amplitude and not in rms. For a given frequency, the orientation of the implanted coil was chosen to produce the maximum H-field normal to the implanted coil, maximizing $\boldsymbol{H}_{\mathbf{max}} \cdot \hat{\boldsymbol{n}}$. The power is a function of the location of the implant depth (z_o) and the distance between the transmitter and the tissue (d_{tx}). Unless otherwise specified, the implant depth is set to $z_o = 3$ cm, and the transmitter distance is $d_{tx} = 1$ cm. The magnetic dipole is arranged to be perpendicular to the tissue surface, analogous to a transmitter coil whose plane is parallel to the tissue surface. In this configuration, there is zero electric field along the axis, where $\theta = 0°$. Therefore, we will assume that the maximum electric field occurs at approximately $\theta = 45°$, at the tissue surface, where $r = \sqrt{2}\, d_{tx}$.

We will consider two possible configurations for the location of the implant relative to the source: $\theta = 0°$ and $\theta = 45°$, referred to as Configuration #1 and Configuration #2, respectively. For Configuration #1 ($\theta = 0)°$, the source-to-implant distance is $r = d_{tx} + z_o$, while for Configuration #2 ($\theta = 45°$), the source-to-implant distance is $r = \sqrt{2}(d_{tx} + z_o)$. Note that in Configuration #1, $\mathbf{H}$ does not contain a 1/r component, while for Configuration #2, there is a 1/r component. In other words, Configuration #1 emphasizes coupling into the evanescent components of the field, while Configuration #2 emphasizes coupling into the radiating components of the field.

The modeling results show that with an implant that contains an air-core coil, the maximum power received at the implant, $P_{r,d}$, exhibits a peak nearly 1 GHz for all tissue types in Configuration #2 [Fig. 5(b), solid line], but there is no clear peak for Configuration #1, which even shows a preference for low frequencies in some tissue types [Fig. 5(a), solid line]. Likewise, when a ferrite core is incorporated, the optimal frequency remains nearly 1 GHz for Configuration #2 [Fig. 5(b), dashed line], but no clear peak is present for Configuration #1 [Fig. 5(a), dashed line). Since the peak power levels are comparable for Configurations #1 and #2, this suggests that there is no clear optimal frequency. These results differ from the plane wave model, illustrating the important role that the evanescent fields play in enhancing power transfer in Configuration #1. Importantly, the peak power that can be achieved for a ferrite core is significantly greater than that of an air core for both Configurations #1 and #2, suggesting that regardless of the frequency of operation, a ferrite core will help to increase the received power.

C. Maximizing Efficiency of the Transmit Link With a Plane Wave Source

In order to optimize for efficiency, we maximize the power received normalized to the total power transmitted. We will approximate the total power transmitted to be the sum of the power received at the implant ($P_{r,p}$), the power absorbed in the tissue (P_{tiss}), and the power dissipated in the core (P_{core})

$$\eta_p = \frac{P_{r,p}}{P_{r,p} + P_{\text{tiss}} + P_{\text{core}}}. \tag{25}$$

An efficiency of $\eta_p = 1$ would indicate that all transmitted power is received at the implant. The expression for the received power for a plane wave source ($P_{r,p}$) is defined in Section III-A. The core loss is defined later, and is generally found to be negligible when compared to the tissue loss ($P_{\text{core}} \ll P_{\text{tiss}}$). Estimating tissue loss involves integrating the power dissipated over the whole volume of tissue

$$P_{\text{tiss}} = \int \frac{1}{2}\sigma_e E^2 dV. \tag{26}$$

To the first order, we can assume most loss occurs at tissue at depths of $z < \delta$. We will approximate the conductivity and the electric field as being uniform over this volume, with an electric field equivalent to the electric field amplitude at the surface of the tissue, E_s. For the plane wave model, the area of tissue exposed to fields is L_o^2, while the volume over which loss occurs is frequency dependent and can be approximated as $\approx L_o^2\delta$. We can express the tissue loss for a plane wave as

$$P_{\text{tiss},p} = \frac{1}{2}\sigma_e E_s^2 L_o^2 \delta, \quad \text{if } \delta < L_o. \tag{27}$$

Equation (27) is valid only for frequencies over which the penetration depth, δ, is less than the total depth of the tissue, L_o. For lower frequencies, where the penetration depth is larger than the tissue length, the total volume considered was L_o^3

$$P_{\text{tiss},p} = \frac{1}{2}\sigma_e E_s^2 L_o^3, \quad \text{if } \delta > L_o. \tag{28}$$

Furthermore, because we are considering far field only for the plane wave source, we can use the wave impedance to express the electric field at the surface, E_s, in terms of the magnetic field at the location of the implant

$$E_s = H(z_o)\sqrt{\mu_o/\epsilon}\, e^{z_o/\delta}. \tag{29}$$

We can now plug in the expressions for received power ($P_{r,p}$) and tissue loss ($P_{\text{tiss},p}$) into the expression for efficiency for a plane wave source (η_p). The amplitude of the magnetic field at the implant, $H(z_o)$, cancels out of this expression, and the efficiency is independent of field level.

The efficiency is plotted across frequency for a range of tissue types both with (dashed line) and without (solid line) a ferrite core [Fig. 6(a)]. With an air core, there is a peak efficiency nearly 1 GHz. With a ferrite core, there is a preference for high frequencies, although a peak cannot be resolved

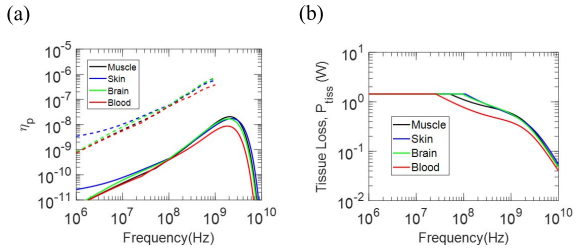

Fig. 6. (a) Efficiency for a plane wave source for various tissue types with a ferrite core (dashed line) and with an air core (solid line). (b) Power dissipated across the whole volume of tissue at the maximum allowed fields set by the SAR limit. The implant coil is a single loop with area $A_{coil} = 0.2$ mm^2, the depth is $z_o = 3$ cm, and the demagnetization factor is $N = 0.08$.

because the ferrites are not characterized above 1 GHz. The absolute value of efficiency is significantly higher with the ferrite core included.

The increase in efficiency over the frequency range of 100 MHz–1 GHz is partly due to the fact that the total tissue loss decreases for increasing frequency over this range [Fig. 6(b)]. This decrease in total power dissipated in the tissue is due to a decrease in penetration depth at higher frequencies. However, this trend is limited at lower frequencies when the penetration depth becomes larger than the depth of the tissue itself. This effect is responsible for the slightly upturn in efficiency at low frequencies, which will become more pronounced in the magnetic dipole model discussed below.

As discussed above, the plane wave model has the advantage of simplicity, but it does not account for any near-field coupling to the transmitter, which will require the use of a magnetic dipole source to account for the impact of both radiating and evanescent fields.

D. Maximizing Efficiency of the Transmit Link With a Magnetic Dipole Source

To estimate efficiency with a magnetic dipole source, we will use a similar approximation that was used for a plane wave source by assuming that the loss occurs primarily within one skin depth of the tissue surface. We will approximate the tissue volume over which loss occurs to be a hemispherical shape with volume

$$V_t = \frac{2}{3}\pi\delta^3, \quad \text{if } \delta < L_o. \tag{30}$$

This expression for volume is valid only for frequencies over which the penetration depth, δ, is less than the total length of the tissue, L_o. For lower frequencies, where the penetration depth is larger than the tissue length, L_o, and the total volume is

$$V_t = \frac{2}{3}\pi L_o^3, \quad \text{if } \delta > L_o. \tag{31}$$

We will assume that the electric field over this volume is approximately constant, taking on a value of the electric field at the surface of the tissue, $|\boldsymbol{E}(r,\theta,\phi)| = |\boldsymbol{E}(d_{tx},0,0)|$. We can approximate the tissue loss for a magnetic dipole source as

$$P_{\text{tiss},d} = \frac{1}{2}\sigma_e V_t |\boldsymbol{E}(d_{tx},0,0)|^2. \tag{32}$$

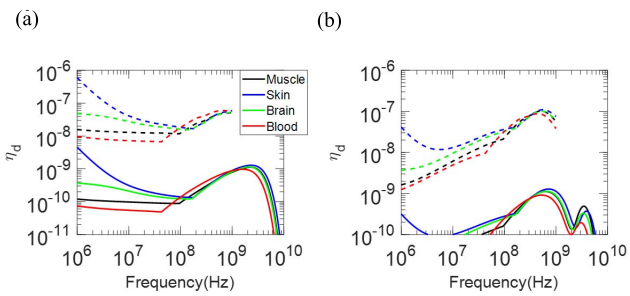

Fig. 7. (a) and (b) Efficiency for a magnetic dipole source for various tissue types with a ferrite core (dashed line) and with an air core (solid line). Results are shown for Configuration #1 in (a) and Configuration #2 in (b). The implant coil is a single loop with area $A_{coil} = 0.2$ mm^2.

We can now define the efficiency for a magnetic dipole source

$$\eta_d = \frac{P_{r,d}}{P_{r,d} + P_{\text{tiss},d} + P_{\text{core}}}. \tag{33}$$

The received power, $P_{r,d}$, is a function of the magnetic field vector at the location of the implant, $\boldsymbol{H}(r,\theta,\phi)$, while the tissue loss, $P_{\text{tiss,d}}$, is given as a function of electric field at the tissue, $\boldsymbol{E}(d_{tx},0,0)$. However, the expressions for magnetic field and electric field are both a function of the amplitude of the magnetic dipole moment, m_o. As a result, m_o cancels out of the expression for efficiency, and the efficiency is not a function of the strength of the applied fields.

The efficiency was estimated for a variety of tissue types for two different locations of the implant: Configuration #1 [Fig. 7(a)] and Configuration #2 [Fig. 7(b)]. As expected, the inclusion of a ferrite core greatly increased the efficiency. For Configuration #2, there is a clear optimal frequency nearly 1 GHz; while for Configuration #1, the results are dependent on tissue type. For muscle and blood, there is a clear advantage to working nearly 1 GHz, while lower frequencies are preferable for skin, and brain shows similar efficiency levels at 1 MHz versus 1 GHz. This suggests that when maximizing efficiency, there is a potential benefit to working in the UHF band.

E. Estimating Core Loss

When an alternating magnetic field is applied to a ferrite core, heat can be generated through hysteresis. If the applied field is sinusoidally oscillating at frequency ω and amplitude H_o, then the power dissipated can be expressed as

$$P_{\text{core}} = Im[\mu]\omega H_o^2 V_{\text{core}} \tag{34}$$

where V_{core} is the volume of the ferrite core, and Im[μ] represents the imaginary component of the permeability [35], [36].

In the analysis above, we stated that the core loss is generally negligible when compared to the tissue loss. To illustrate this, we compared the power dissipation [Fig. 8(a) and (b)] and the power density [Fig. 8(c) and (d)] of the ferrite core versus the tissue loss for muscle. The source was a magnetic dipole, with the implant location relative to the transmitter defined by Configuration #2. The applied field levels were set to the maximum allowed by the SAR limit. Clearly, the core loss is negligible compared to the tissue loss for the nominal

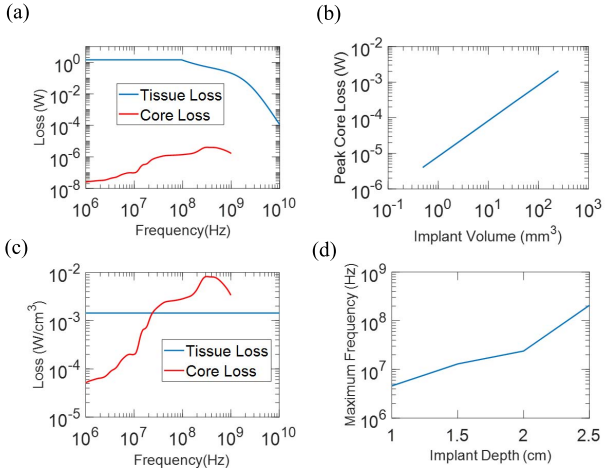

Fig. 8. (a) Power loss generated in the ferrite core (red) and the tissue (blue), assuming a cylindrical core with diameter and length of 0.5 and 2.5 mm, respectively. (b) Peak core loss, measured across a range of frequencies of 1 MHz–1 GHz, plotted versus implant volumes. (c) Power density associated with core loss (red) and tissue loss (blue). (d) Maximum frequency represents the frequency above which the core loss exceeds the tissue loss. The source was a magnetic dipole in Configuration #2. The implant depth was $z_o = 2$ cm for (a)–(c).

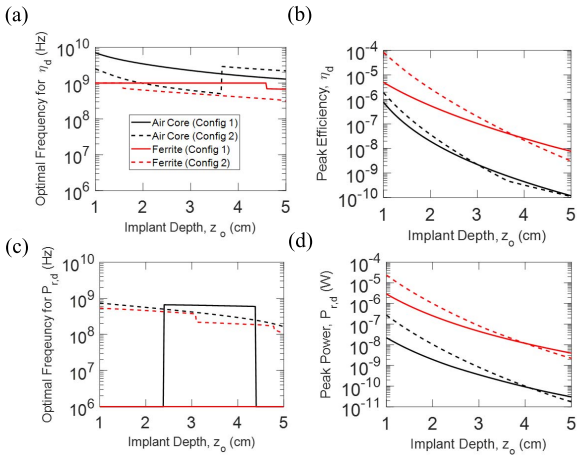

Fig. 9. Optimal frequency and peak value of efficiency (a and b) and power (c and d) are shown, with an air and a ferrite core, over a range of implant depths. The frequencies were constrained to <1 GHz when ferrite cores were included, and <10 GHz when an air core was used. Results are for a magnetic dipole source with muscle tissue, assuming an implant location defined by either Configuration #1 or #2. The diameter and length of the ferrite core were 0.5 and 2.5 mm, respectively (N = 0.08).

device consisting of a cylindrical core with diameter, length, and volume of 0.5, 2.5, and 0.5 mm^3, respectively [Fig. 8(a)]. Next, the volume of the implant was increased and the peak heating that was observed across frequency (1 MHz–1 GHz) [Fig. 8(b)]. For increasing volume size, we maintained the aspect ratio at 5:1 in order to ensure the demagnetization factor remained unchanged at N = 0.08. Only for relatively large volumes exceeding 100 mm^3 does the peak heating of the core begin to approach the magnitude of the tissue loss, suggesting that efficiency will be largely unaffected by core loss.

Aside from efficiency, another consideration is whether the core loss can generate power density levels that are unsafe for the surrounding tissue. This will depend partly on the thermal design of the device, and its ability to redirect or absorb heat generated from the core and prevent it from reaching the tissue. But in order to keep the analysis simple, we will assume that unsafe levels will occur when the heat density levels from the core, in W/cm^3, approach that of the tissue heating at field levels set by the SAR limit.

We show that the core loss density generally increases with frequency while the tissue loss density remains relatively flat at ≈1 mW/cm^3, a level determined by the SAR limit [Fig. 8(c)]. For an implant depth of $z_o = 2$ cm, the power density associated with core loss will exceed that of the tissue loss for frequencies above 20 MHz. Such heat could potentially be unsafe if this excess heat was to flow into the tissue, and therefore, we define a maximum frequency of safe operation. This maximum frequency is not dependent on volume, but it is dependent on implant depth [Fig. 8(d)]. For shallower implants, the magnetic field impinging on the core is larger than for deeper implants, and thus, the core loss is greater for shallow implants, bringing the maximum frequency lower. For example, at 1.5 cm depth, the maximum frequency is ∼10 MHz, suggesting that the frequencies should be kept below 10 MHz in order to ensure the power density generated in the core remains below that of the tissue loss. For implant depths >2.5 cm, the heat density levels were below the tissue heating for all frequencies. This suggests that for very shallow implants (<2.5 cm), the optimal frequency of operation can be constrained by the heating of the core rather than by direct heating of the tissue.

F. Effect of Implant Depth (z_o) on Efficiency and Power

To examine the effect of implant depth (z_o) on efficiency (η_d) and received power (P_{rd}), we varied the depth from 1 to 5 cm, using a magnetic dipole source. The implant location relative to the transmitter is defined by Configurations #1 and #2, defined above. The optimal frequency for efficiency was found to be relatively high for both Configurations #1 and #2 (>300 MHz), showing a slight decrease for deeper implants [Fig. 9(a)]. The abrupt transitions in optimal frequency resulted from the fact that the efficiency versus frequency curves exhibited multimodal peaks whose relative amplitudes varied with implant depth. Across all implant depths, the presence of a ferrite core resulted in a significant increase in the overall efficiency of the link as compared to an air core [Fig. 9(b)]. For shallow implants (<3 cm), there was a significant benefit to working on Configuration #2, where the 1/r component of the H-field contributed to power transfer.

For maximizing power transfer (P_{rd}) rather than efficiency (η_d), the optimal frequency was found to depend strongly on the position of the implant [Fig. 9(c)]. In Configuration #2, where the 1/r component of the H-field contributed to power transfer, frequencies in the UHF band were optimal. But for Configuration #1, where the power was transferred only through the 1/r^2 and 1/r^3 components of the H-field, the optimal frequency was as low as possible over the frequency range evaluated (≥1 MHz). Importantly, the peak power transferred was comparable between Config-

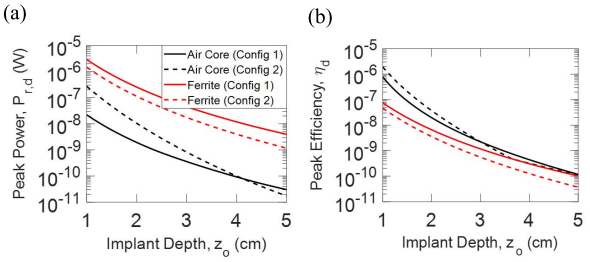

Fig. 10. Peak value of (a) received power and (b) efficiency, with an air and ferrite core, over a range of implant depths. To minimize core heating, the frequencies were constrained to <10 MHz when ferrite cores were included, while frequencies of <10 GHz were used for an air core. Results are for a magnetic dipole source with muscle tissue, assuming an implant location defined by either Configuration #1 or #2. The diameter and length of the ferrite core were 0.5 and 2.5 mm, respectively (N = 0.08).

urations #1 and #2 at implant depths of 3–5 cm [Fig. 9(d)], suggesting that there is no significant benefit to working at low versus high frequencies for optimizing received power. As with efficiency, shallow implants showed a slight preference for Configuration #2. The overall power transfer was greatly increased when a ferrite core was included for both configurations as compared to an air core.

Next, we considered the case where the heating was minimized by operating the ferrite core at lower frequencies (<10 MHz). Note that heating only reaches unsafe levels for shallow implants and relatively high field strengths (Fig. 8). We will compare two cases: 1) the ferrite core is powered at frequencies spanning 1–10 MHz and 2) the air core is powered at frequencies spanning 1 MHz to 10 GHz. The peak received power and efficiency were plotted in Fig. 10. These results show an increase in the peak received power that can be achieved by using a ferrite core as compared to an air core, even when the ferrite is powered at low frequencies [Fig. 10(a)]. Interestingly, the peak efficiency is greater with the air core than the ferrite core, at least for shallow implants [Fig. 10(b)]. This suggests that there is a particular application where air cores would be beneficial over ferrite cores; namely, for shallow implants and high field levels where efficiency takes priority over received power.

IV. Discussion

The model presented provides a framework for assessing the impact of a ferrite core on the performance and safety of wirelessly powered implantable devices. For maximizing efficiency, the optimal frequency with a ferrite core remains in the UHF band, although results depend strongly on tissue composition. Conversely, when maximizing received power rather than efficiency, the results depend on the source. For a plane wave source, the optimal frequency for received power remains in the UHF band with a ferrite core. However, for a magnetic dipole source, there was no clear optimal frequency, yielding comparable power transfer at 1 MHz and 1 GHz. Because the magnetic dipole source accounts for both the evanescent and radiating components of the source, this model more accurately represents the transmitter for biological applications. Therefore, these results show that: 1) maximizing power transfer does not exhibit a clear optimal frequency and 2) the near-field components of the source play a critical role in enhancing the power transfer at low frequencies.

A. Applications of Ferrites for Wireless Power Transfer to Implantable Devices

One example where ferrite cores could find use is in the ultraminiaturization of medical implants. Such devices are finding expanding applications in neural stimulation, drug delivery, and blood glucose monitoring [37]–[39]. When device size is on the order of ≈1 mm^3, it becomes difficult to deliver sufficient wireless power to operate the device, and therefore maximizing the total power delivered becomes critical. Previous modeling work shows the large boost in power transfer that is associated with the inclusion of a ferrite [10], [40], [41]. In these applications, the benefits of ferrite cores must be weighed against the associated MRI restrictions. Depending on the size of the core and the field levels of the scanner, such implants can be safe for MRI use, although they can cause image artifacts near the implant [42].

Another example where ferrite cores could find use is in decreasing the recharge time of implantable batteries. Primary cell batteries will continue to be used for life-critical applications, such as pace makers, but there are many applications where rechargeable (secondary) batteries find use as well [43]. For example, there are several emerging areas of therapy that involve neural stimulation that requires implantable batteries. Decreasing the recharge time with a ferrite core could help with patient compliance, and could influence the manufacturers or clinician's decision on whether the secondary battery would be a better choice than primary cells.

There are other factors besides efficiency and power transfer that must be taken into account when designing a full wireless system. For example, lower frequencies will generally involve higher field levels, necessitating higher current levels. This can lead to larger power amplifiers and heat sinks that preclude their use as wearable transmitters, such as those used to power implantable neural stimulators for treating pain [44]. These issues can be mitigated at higher frequencies, where the transmitter could be made lightweight and even wearable. However, the downside of very small transmitters is that the power delivery will be very sensitive to the position of the transmitter. For example, if the implant and the transmitter are both on the order of 1 cm^3, then even small movements of the transmitter can result in large changes in field levels at the implant. In contrast, an inductive link could involve a large (>5 cm) transmit coil, yielding a link that is relatively insensitive to transmitter position, although it would be sensitive to the relative orientation of the coils. These tradeoffs must be considered for each specific application.

B. Limitations to the Model

There are some limitations to the model presented here. First, we considered the tissue to have homogeneous electrical properties rather than incorporating different layers of tissue into the model (e.g., skin, fat, and muscle layers). Second,

we did not incorporate the properties of air between the transmitter and tissue. These two approximations allowed us to derive simple analytical expressions for efficiency and received power, which is not trivial for a multilayered structure with a source region around the transmitter. The design of any specific implantable system would likely involve finite element modeling, which allows easy incorporation of these effects, including any dispersive properties of the tissue. Therefore, we consider any errors associated with these approximations to be a worthwhile tradeoff for achieving a simple, analytical model. Third, we do not answer what is the theoretical limit of maximum power transfer that can be delivered for a given volume of the implanted device. Answering this question would require an exploration of a number of factors, including the size and shape of the implant, the number of turns in the implanted coil, the size of the transmitter, the matching network, and the particular type of ferrite being employed.

Finally, because the model presented here is intended to be independent of the specific design of the implanted device, we did not include any detailed analysis on the winding loss or matching network [45]. The winding loss can become appreciable in the UHF band, and therefore should be accounted for in the design of an implant once its size and materials are established. In terms of matching, our model assumed a conjugate-matched network, yielding a frequency-independent (real-valued) load impedance. In reality, there will be some frequency dependence associated with this matching network that will depend on many factors, such as size of the implanted coil and any size restrictions on the matching network. This matching can become complex because it involves not only the self-inductance of the implanted coil but also coupling between the transmitter and implanted coil. Such coupling could be via pure mutual inductance at lower frequencies [46], as well as more complex interactions higher frequencies where midfield coupling occurs [7]. Further work will be needed to evaluate the impact of the matching network on the optimal frequency for the case when the implant includes a ferrite core.

V. Conclusion

A simple theoretical model is presented that provides a framework for assessing the impact that a ferrite core will have on the wireless power transfer to implantable devices. We illustrate the importance of distinguishing designs optimized for efficiency—i.e., minimizing the transmitter power for a given received power—from designs optimized for received power—i.e., maximizing received power within the SAR limit. The model results suggest that when a ferrite core is incorporated into the implant, the optimal frequency for efficiency remains at relatively high frequencies, in the UHF band. Conversely, when optimizing for received power, there is little benefit to working at UHF versus traditional inductive coupling at lower frequencies.

Acknowledgment

The authors would like to thank R. McNabb and M. Weinberg for their helpful input during the preparation of this paper.

References

[1] M. Baker and R. Sarpeshkar, "Feedback analysis and design of RF power links for low-power bionic systems," *IEEE Trans. Biomed. Circuits Syst.*, vol. 1, no. 1, pp. 28–38, Mar. 2007.

[2] H. Cao *et al.*, "An implantable, batteryless, and wireless capsule with integrated impedance and pH sensors for gastroesophageal reflux monitoring," *IEEE Trans. Biomed. Eng.*, vol. 59, no. 11, pp. 3131–3139, Nov. 2012.

[3] M. Zargham and P. G. Gulak, "Maximum achievable efficiency in near-field coupled power-transfer systems," *IEEE Trans. Biomed. Circuits Syst.*, vol. 6, no. 3, pp. 228–245, Jun. 2012.

[4] H.-M. Lee and M. Ghovanloo, "A power-efficient wireless capacitor charging system through an inductive link," *IEEE Trans. Circuits Syst. II, Exp. Briefs*, vol. 60, no. 10, pp. 707–711, Oct. 2013.

[5] K. Agarwal, R. Jegadeesan, Y.-X. Guo, and N. V. Thakor, "Wireless power transfer strategies for implantable bioelectronics," *IEEE Rev. Biomed. Eng.*, vol. 10, pp. 136–161, Mar. 2017. doi: 10.1109/RBME.2017.2683520.

[6] Y. Cheng, G. Wang, and M. Ghovanloo, "Analytical modeling and optimization of small solenoid coils for millimeter-sized biomedical implants," *IEEE Trans. Microw. Theory Techn.*, vol. 65, no. 3, pp. 1024–1035, Mar. 2017.

[7] A. S. Y. Poon, S. O'Driscoll, and T. H. Meng, "Optimal frequency for wireless power transmission into dispersive tissue," *IEEE Trans. Antennas Propag.*, vol. 58, no. 5, pp. 1739–1750, May 2010.

[8] J. S. Ho and A. S. Y. Poon, "Energy transfer for implantable electronics in the electromagnetic midfield," *Prog. Electromagn. Res.*, vol. 148, pp. 151–158, May 2014.

[9] D. Nikolayev, M. Zhadobov, M. Karban, and R. Sauleau, "Electromagnetic radiation efficiency of body-implanted devices," *Phys. Rev. Appl.*, vol. 9, no. 2, 2018, Art. no. 024033.

[10] D. Freeman *et al.*, "A sub-millimeter, inductively powered neural stimulator," *Frontiers Neurosci.*, vol. 11, p. 659, Nov. 2017.

[11] J. C. Schuder and H. E. Stephenson, "Energy transport to a coil which circumscribes a ferrite core and is implanted within the body," *IEEE Trans. Biomed. Eng.*, vol. BME-12, nos. 3–4, pp. 154–163, Jul./Oct. 1965.

[12] P. T. Theilmann and P. M. Asbeck, "An Analytical model for inductively coupled implantable biomedical devices with ferrite rods," *IEEE Trans. Biomed. Circuits Syst.*, vol. 3, no. 1, pp. 43–52, Feb. 2009.

[13] A. J. Hanson, J. A. Belk, S. Lim, D. J. Perrault, and C. R. Sullivan, "Measurements and performance factor comparisons of magnetic materials at high frequency," in *Proc. IEEE Energy Convers. Congr. Expo. (ECCE)*, Sep. 2015, pp. 5657–5666.

[14] *C95.1-1991–IEEE Standard for Safety Levels with Respect to Human Exposure to Radio Frequency Electromagnetic Fields, 3 kHz to 300 GHz*, IEEE Standard C95.1, 2005.

[15] S. Gabriel, R. W. Lau, and C. Gabriel, "The dielectric properties of biological tissues: III. Parametric models for the dielectric spectrum of tissues," *Phys. Med. Biol.*, vol. 41, no. 11, p. 2271, 1996.

[16] C. Gabriel, S. Gabriel, and E. Corthout, "The dielectric properties of tissues and biological tissues: I. Literature survey," *Phys. Med. Biol.*, vol. 41, no. 11, p. 2231, 1996.

[17] K. R. Foster and H. P. Schwan, "Dielectric properties of tissues and biological materials: A critical review," *Critical Rev. Biomed. Eng.*, vol. 17, no. 1, pp. 25–104, 1989.

[18] R. D. Stoy, K. R. Foster, and H. P. Schwan, "Dielectric properties of mammalian tissues from 0.1 to 100 MHz: A summary of recent data," *Phys. Med. Biol.*, vol. 27, no. 4, pp. 501–513, 1982.

[19] H. P. Schwan, "Electrical properties of tissue and cell suspensions," *Adv. Biol. Med. Phys.*, vol. 5, pp. 147–209, Jan. 1957.

[20] J. G. Schuder, J. H. Gold, and H. E. Stephenson, "An inductively coupled RF system for the transmission of 1 kW of power through the skin," *IEEE Trans. Biomed. Eng.*, vol. BME-18, no. 4, pp. 265–273, Jul. 1971.

[21] W. H. Ko, S. P. Liang, and C. D. F. Fung, "Design of radio-frequency powered coils for implant instruments," *Med. Biol. Eng. Comput.*, vol. 15, no. 6, pp. 634–640, 1977.

[22] M. Soma, D. C. Galbraith, and R. L. White, "Radio-frequency coils in implantable devices: Misalignment analysis and design procedure," *IEEE Trans. Biomed. Eng.*, vol. BME-34, no. 4, pp. 276–282, Apr. 1987.

[23] W. J. Heetderks, "RF powering of millimeter- and submillimeter-sized neural prosthetic implants," *IEEE Trans. Biomed. Eng.*, vol. 35, no. 5, pp. 323–327, May 1988.

[24] V. Raicu and Y. Feldman, *Dielectric Relaxation in Biological Systems*. Oxford, U.K.: Oxford Univ. Press, 2015.

[25] D. J. Griffiths, *Introduction to Electrodynamics*. Upper Saddle River, NJ, USA: Prentice-Hall, 1998.
[26] N. Hamilton, "The small-signal frequency response of ferrites," *High Freq. Electron., Summit Tech. Media*, vol. 10, pp. 36–52, 2011.
[27] D. Jiles, *Introduction to Magnetism and Magnetic Materials*. London, U.K.: Taylor & Francis, 1998.
[28] E. Purcel and D. Morin, *Electricity and Magnetism*, 3rd ed. Cambridge, U.K.: Cambridge Univ. Press, 2014.
[29] M. Wang, J. Feng, Y. Shi, and M. Shen, "Demagnetization weakening and magnetic field concentration with ferrite core characterization for efficient wireless power transfer," *IEEE Trans. Ind. Electron.*, vol. 66, no. 3, pp. 1842–1851, Mar. 2018.
[30] S. Tumanski, "Induction coil sensors—A review," *Meas. Sci. Technol.*, vol. 18, no. 3, p. 31, 2007.
[31] M. Sato and Y. Ishii, "Simple and approximate expressions of demagnetizing factors of uniformly magnetized rectangular rod and cylinder," *J. Appl. Phys.*, vol. 66, no. 983, pp. 983–985, 1989.
[32] T. Allen, H. Krzywicki, and J. E. Roberts, "Density, fat, water and solids in freshly isolated tissues," *J. Appl. Phys.*, vol. 14, no. 6, pp. 1005–1008, 1959.
[33] K. Psathas, A. Kiourti, and K. S. Nikita, *Safety Issues in Biomedical Telemetry*. Hoboken, NJ, USA: Wiley, 2014.
[34] M. Sadiku, *Elements of Electromagnetics*, 6th ed. Oxford, U.K.: Oxford Univ. Press, 2014.
[35] X. Nan and C. R. Sullivan, "A two-dimensional equivalent complex permeability model for round-wire windings," in *Proc. IEEE 36th Power Electron. Specialist Conf.*, Jun. 2005, pp. 613–618.
[36] R. E. Rosensweig, "Heating magnetic fluid with alternating magnetic field," *J. Magn. Mater.*, vol. 252, pp. 370–374, Nov. 2002.
[37] S. H. Lee *et al.* "Implantable batteryless device for on-demand and pulsatile insulin administration," *Nature Commun.*, vol. 13, no. 8, 2017, Art. no. 15032.
[38] Y. Ma, Z. Luo, C. Steiger, G. Traverso, and F. Adib, "Enabling deep-tissue networking for miniature medical devices," in *Proc. ACM SIGCOMM*, Budapest, Hungary, 2018, pp. 417–431.
[39] J. Y. Lucisano, T. L. Routh, J. T. Lin, and D. A. Gough, "Glucose monitoring in individuals with diabetes using a long-term implanted sensor/telemetry system and model," *IEEE Trans. Biomed. Eng.*, vol. 64, no. 9, pp. 1982–1993, Sep. 2017.
[40] T. P. Delhaye, N. André, S. Gilet, C. Gimeno, L. A. Francis, and D. Flandre, "High-efficiency wireless power transfer for mm-size biomedical implants," in *Proc. IEEE Sensors*, Glasgow, U.K, Nov. 2017, pp. 1–3.
[41] R. Carta *et al.*, "Wireless powering for a self-propelled and steerable endoscopic capsule for stomach inspection," *Biosensors Bioelectron.*, vol. 25, pp. 845–851, Dec. 2009.
[42] F. G. Shellock, G. Cosendai, S. M. Park, and J. A. Nyenhuis, "Implantable microstimulator: Magnetic resonance safety at 1.5 Tesla," *Invest Radiol.*, vol. 39, no. 10, pp. 591–599, 2004.
[43] D. C. Bock, A. C. Marschilok, K. J. Takeuchi, and E. S. Takeuchi, "Batteries used to power implantable biomedical devices," *Electrochimica Acta*, vol. 84, pp. 155–164, Dec. 2013.
[44] K. V. Slavin, "Stimulation of the peripheral nervous sysytem: The neuromodulation frontier," *Prog. Neurol. Surgery*, vol. 29, pp. 168–191, 2016. [Online]. Available: https://www.karger.com/Article/Pdf/434702
[45] A. Yakovlev, S. Kim, and A. Poon, "Implantable biomedical devices: Wireless powering and communication," *IEEE Commun. Mag.*, vol. 50, no. 4, pp. 152–159, Apr. 2012.
[46] Z. Miao, D. Liu, and C. Gong, "Efficiency enhancement for an inductive wireless power transfer system by optimizing the impedance matching networks," *IEEE Trans. Biomed. Circuits Syst.*, vol. 11, no. 5, pp. 1160–1170, Oct. 2017.
[47] J. S. Ho *et al.*, "Wireless power transfer to deep-tissue microimplants," *Proc. Nat. Acad. Sci.*, vol. 111, no. 22, pp. 7974–7979, 2014.
[48] D. W. Perry, D. B. Grayden, R. K. Shepherd, and J. B. Fallon, "A fully implantable rodent neural stimulator," *J. Neural Eng.*, vol. 9, no. 1, 2012, Art. no. 014001.
[49] R. E. Millard and R. K. Shepherd, "A fully implantable stimulator for use in small laboratory animals," *J. Neurosci. Methods*, vol. 166, no. 2, pp. 168–177, 2007.
[50] M. Manoufali, K. Bialkowski, B. Mohammed, and A. Abbosh, "Wireless power link based on inductive coupling for brain implantable medical devices," *IEEE Antennas Wireless Propag. Lett.*, vol. 17, no. 1, pp. 160–163, Jan. 2018.

Daniel K. Freeman received the Ph.D. degree in biomedical engineering from Boston University, Boston, MA, USA, in 2008.

He was a Post-Doctoral Fellow at the Massachusetts Institute of Technology, Cambridge, MA, USA, and Harvard Medical School, Boston, MA, USA. He is currently a Member of Technical Staff at the MIT Lincoln Laboratory, Lexington, MA, USA. His past research interests include retinal implants, cold cathode vacuum amplifiers, MEMS electric and magnetic field sensors, and biophysical modeling of the electrical stimulation of cells, such as neural implants and electroporation.

Steven J. Byrnes received the B.A. degree *(summa cum laude)* in physics from Harvard University, Cambridge, MA, USA, in 2007, and the Ph.D. degree in physics from the University of California at Berkeley, Berkeley, CA, USA, in 2012.

He held a post-doctoral position at the Capasso Laboratory, Harvard University, where he was involved in optical physics and optoelectronics. Since 2015, he has been with the Advanced Instrumentation Group, Draper, Cambridge, MA, USA, where he specializes in physics-based design and analysis. He has helped develop a wide variety of sensors and systems from medical imaging and LIDAR to electronic devices and atomic clocks.